analytical chemistry

Article

pubs.acs.org/ac

Microfluidic Integration of Parallel Solid-Phase Liquid Chromatography

Jens Huft,[†,‡] Charles A. Haynes,[§] and Carl L. Hansen*[,†,#]

[†]Centre for High-Throughput Biology, University of British Columbia, Vancouver BC, Canada

[‡]Department of Electrical and Computer Engineering, University of British Columbia, Vancouver BC, Canada

[§]Department of Chemical and Biological Engineering, University of British Columbia, Vancouver BC, Canada

[#]Department of Physics and Astronomy, University of British Columbia, Vancouver BC, Canada

Supporting Information

ABSTRACT: We report the development of a fully integrated microfluidic chromatography system based on a recently developed column geometry that allows for robust packing of high-performance separation columns in poly(dimethylsiloxane) microfluidic devices having integrated valves made by multilayer soft lithography (MSL). The combination of parallel high-performance separation columns and on-chip plumbing was used to achieve a fully integrated system for on-chip chromatography, including all steps of automated sample loading, programmable gradient generation, separation, fluorescent detection, and sample recovery. We demonstrate this system in the separation of fluorescently labeled DNA and parallel purification of reverse transcription polymerase chain reaction (RT-PCR) amplified variable regions of mouse immunoglobulin genes using a strong anion exchange (AEX) resin. Parallel sample recovery in an immiscible oil stream offers the advantage of low sample dilution and high recovery rates. The ability to perform nucleic acid size selection and recovery on subnanogram samples of DNA holds promise for on-chip genomics applications including sequencing library preparation, cloning, and sample fractionation for diagnostics.

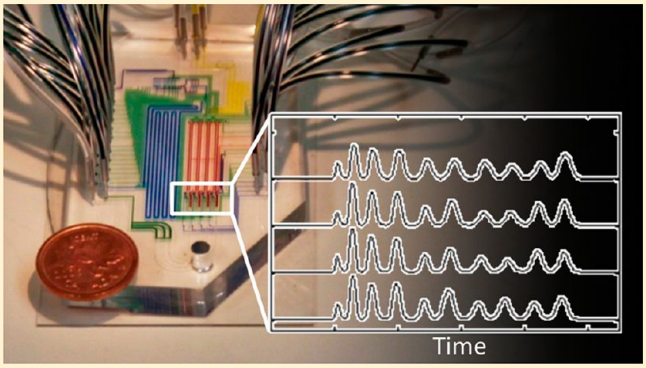

Microfluidic systems offer inherent advantages of small volume processing, excellent reproducibility, minimal dead-volume, and automation, making them attractive platforms for the miniaturization and integration of biochemical analysis.[1−7] One long-standing objective has been the integration of macromolecule separations on chip,[8] an application that directly benefits from low dilution, precise sample injection, and higher detection sensitivity.[9,10] Due to their ease of integration, microfluidic electrophoretic systems have been developed extensively and are available as commercial instruments for the analysis of proteins and nucleic acids.[11−13] By comparison, the integration of complete solid-phase liquid chromatography systems has remained elusive, owing both to the increased complexity of separation protocols and technical challenges in the microfabrication of chromatography columns on chip.

Solid-phase chromatography is an extremely versatile separation technique in which a sample interacts with a packed column of functionalized resin under changing buffer conditions designed to differentially modulate the affinity and, hence, the mobility of each species in the mixture. Changing the physical and chemical properties of the resin allows for a large variety of separation modalities including ion exchange, reverse phase, affinity, and size exclusion. The importance of this method has resulted in the development and availability of a myriad of resin technologies that are optimized for specific separation applications and modalities. Thus, the integration of chromatography in a microfluidic format would greatly enhance the flexibility and performance of on-chip separation applications.

Implementing solid-phase chromatography in a microfluidic format requires the combined capabilities of reliable packing of high-quality microcolumns with resin, on-chip gradient generation, and multistep sample processing that includes loading, washing, and recovery. While the fabrication of solid-phase microcolumns has been demonstrated in materials with a high Young's Modulus such as glass, silicon, or polyimide,[14−18] these materials are not easily amenable to microvalve integration. This, coupled with low yield in column packing, has limited the level of on-chip integration and parallelization achieved to date.[19−21]

To lift this restriction, we recently developed a novel column geometry that allows for the parallel packing of high-quality microfluidic separation columns within minutes and with exceptional yield and reproducibility.[22] Importantly, this low-

Received: January 16, 2013
Accepted: February 5, 2013
Published: February 5, 2013

   dx.doi.org/10.1021/ac400163u | *Anal. Chem.* 2013, 85, 2999−3005

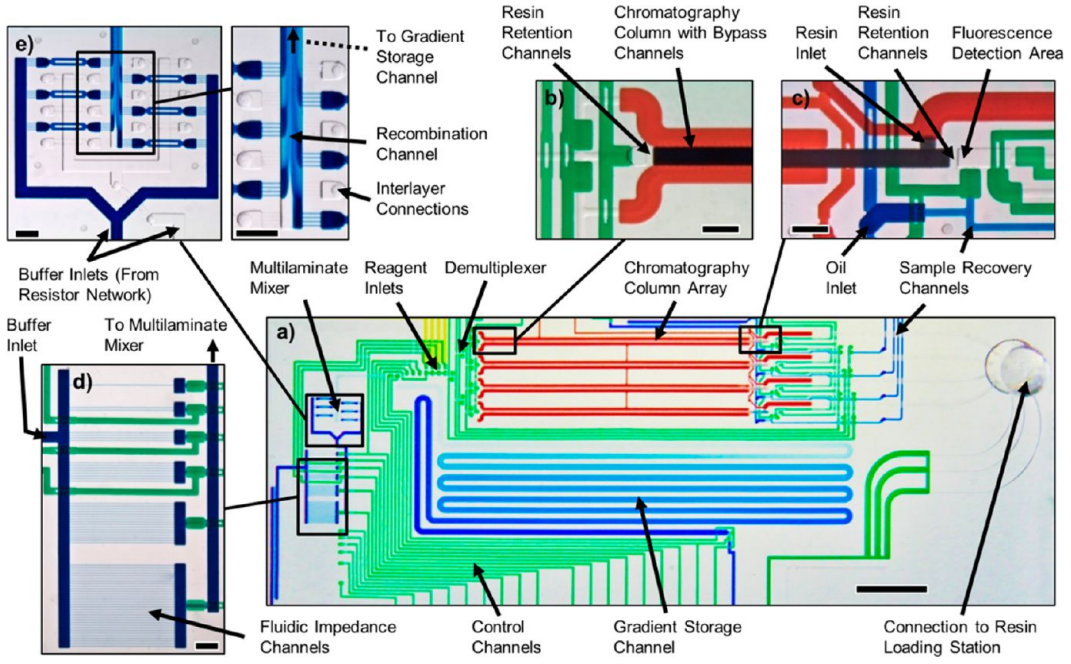

Figure 1. Integrated microfluidic chromatography system. (a) Micrograph of a microfluidic device with elements for column packing, sample loading, gradient generation, and sample recovery. For visualization, valves and various channel sections have been filled with dye: column valves (red), valves for device operation (green), reagent inlets (yellow), buffer B inlet with impedance network (blue), gradient storage channel (gradient blue), oil inlet for sample recovery (blue). (b) Micrograph of the front of one of the four chromatography columns. (c) Micrograph of the back of the same column as shown in (b) with the column outlet separated from the oil channel (blue) by a closed valve (green). (d) Micrograph of one of the two impedance networks for gradient generation. (e) Micrograph of the multilaminate mixer interlacing flow streams of low and high salt concentration buffers. The inset shows the mixing channel with partly mixed dyes. The scale bars are 50 mm (a) and 400 μm (b–e), respectively.

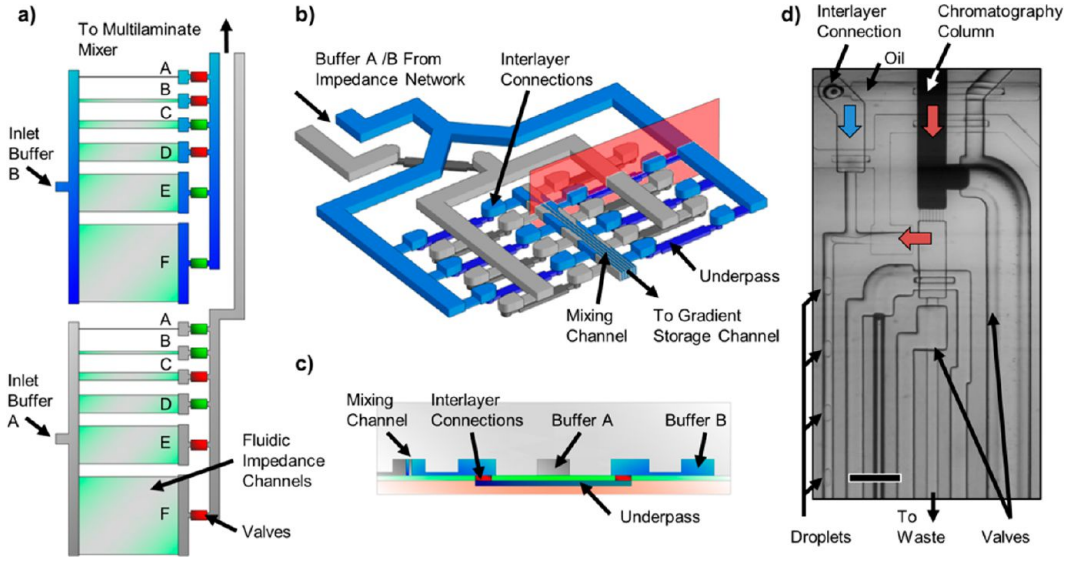

Figure 2. (a) Schematic of the impedance network for gradient generation: each of the two resistor banks (one for each buffer) consists of six sets of channels (A–F) with the following fluidic impedances: $R = 7 \times 10^{16}$ Pa s/m^3 (A), $R/2$ (B), $R/4$ (C), $R/8$ (D), $R/16$ (E), $R/32$ (F). Valve states for each set are chosen in a complementary fashion that preserves the total flow rate such that any combination of one resistor network is reversed in the other set. (b) Schematic of the multilaminate mixer: a mixing time of 1s is achieved by splitting each of the two buffer streams into six streams which are interlaced in an alternating fashion using interlayer connections and joined in a single channel. (c) Schematic of the cross-section indicated in (b) showing one of the 12 underpasses and two of the interlayer connections. (d) Micrograph of the back of one of the four columns. The flow direction of the eluent and the oil are indicated by red and blue arrows, respectively. With only one of the valves open, the aqueous eluent is injected into the flow stream of an immiscible oil phase. Droplets of the recovered fraction are pooled for recovery. The scale bar is 400 μm.

pressure packing method is compatible with poly(dimethylsiloxane) (PDMS) microfluidic devices with integrated microvalves made by multilayer soft lithography (MSL). Briefly, rapid and low-pressure packing is achieved using a column geometry that features arrays of bypass channels located all along the length of the column. During the packing process, these channels provide a low-impedance path for the resin slurry solvent, thereby allowing for high flow rates via

dx.doi.org/10.1021/ac400163u | *Anal. Chem.* 2013, 85, 2999–3005

lateral flow. Following packing, these bypass channels are closed using microvalves to create a standard column geometry with a single inlet and outlet at either end of the separation channel.

Here, we build on this fabrication method to achieve the first completely integrated solid-phase chromatographic system on a PDMS microdevice. MSL-based fluidics are used to implement all elements required for chromatographic separation including resin loading, column packing, sample injection, programmable gradient generation, parallel sample separation, and automated fraction recovery with high precision and yield. We highlight the application of these capabilities in genomics applications by performing a variety of on-chip nucleic acid separations using strong anion exchange (AEX) chromatography.

DEVICE FABRICATION AND LAYOUT

Fabrication. PDMS microfluidic devices with integrated membrane valves were made using a modified version of the MSL process.[23,24] Modifications to the original MSL protocol include the bonding of consecutive layers using oxygen plasma activation and the creation of layer−layer interconnects using laser ablation.[25] Details of device fabrication are provided as Supporting Information.

Column Packing. A fully integrated microdevice for liquid chromatography is shown in Figure 1. Each chromatography column is 20 mm long and lined by 520 trap channels along the long edges of the column (Figure 1b,c). The height of the trap channels is smaller than the diameter of the chromatography beads, allowing the solvent of the chromatography resin slurry to flow laterally through the sides of the column while retaining the chromatography beads within the column volume. Due to the relatively low flow impedance during the packing process, multiple columns can be packed simultaneously within less than 10 min at a pressure of 207 kPa (30 psi). During packing, the array of chromatography columns is connected to an external resin loading station which keeps the insoluble AEX beads (Proteomix 5 μm nonporous, Sepax Technologies, DE) in suspension and allows for a rapid injection of the resin slurry into the chromatography columns. Columns are packed in reverse; the resin inlet is located at the back of the column. This method was found to improve packing density and homogeneity at the column inlet, allowing the sample to bind in a tight band to the chromatographic resin upon loading. Potential resin imperfections are located at the column outlet, where their influence on the separation is minimal. Upon completion of the packing process, the waste flow channels are sealed, isolating columns from each other.

Gradient Generation. Our device includes an integrated gradient generator to allow for user-programmable modulation and optimization of buffer conditions during sample separation (Figure 2a). Defined buffer gradient profiles are created using valves to modulate the relative flow of two buffers, designed to favor binding or elution of the sample from the column. This gradient is created prior to separation and stored in a holding line that is then connected to the column inlet using microvalves to reconfigure the flow path. The gradient generator works by changing the relative flow impedance for each buffer using two identical sets of variable fluidic resistors. Each resistor bank consists of six individually addressable fluidic resistors, connected in parallel and having impedances of R, $R/2$, $R/4$, $R/8$, $R/16$, and $R/32$. The selection of different combinations of these resistors allows for the modulation of the total resistance over 64 discrete levels, effectively implementing a 6-bit "digitization" of the flow rate. During gradient formation, the valve states for each resistor bank are operated in a complementary fashion that preserves the total flow rate; any combination of one resistor network is reversed in the other set. For AEX separation of nucleic acids, the two buffers to be mixed were a low salt buffer A (0.6 M NaCl, 25 mM Tris, 1 mM EDTA, 0.1% Tween, 15 mM NaN_3) and a high salt buffer B (A with 0.8 M NaCl).

In addition to NaCl gradients, we have successfully generated low-concentration methanol gradients with complementary resistor banks for the use in reverse-phase applications. However, we note that prolonged exposure of PDMS to some gradient components such as high-concentration methanol, acetonitrile, or acid modifiers may result in significant material swelling or the leaching of uncured monomers. Thus, although our gradient generation method is general, the use of PDMS devices may be restrictive in some applications. In such cases it may be necessary to develop processes for the coating of PDMS or to use alternative elastomers.[26]

Multilaminate Mixer. In order to ensure complete mixing of the two buffers, a multilaminate mixer is incorporated between the gradient generator and the gradient storage line (Figure 2b). Each of the two inlet channels is split into 6 streams which are interlaced in an alternating fashion using interlayer connections and joined in a single channel.[25] This format reduces the mixing time to 1 s and ensures that no lateral concentration gradients persist across the width of the storage channel. We note that under appropriate operating conditions this mixing functionality may not be essential as diffusion is sufficient to relax any lateral gradients during gradient storage; nevertheless, the inclusion of the mixer offers several advantages including equalizing dispersion effects for the two streams, allowing for the use of higher flow rates during gradient formation, and enabling the use of wider storage channels. After passing through the multilaminate mixer, the gradient is directed to a storage channel which holds the entire gradient before it is applied to the chromatography columns. We found that directly applying the gradient to the high-impedance columns (as opposed to first storing it) is generally less reliable as the buffer flow is pressure driven and minor fluctuations in the input pressure of one of the two buffers results in buffer back-flow through the resistor bank with the lower pressure.

Sample Loading and Recovery. As each of the four parallel columns (Figure 1) is individually addressable through a bifurcated channel structure, up to four different samples can be loaded following column preparation by regeneration with a high-salt buffer and equilibration with a low-salt buffer. The gradient is then applied to either one or multiple columns, thereby allowing for parallel operation or sequential operation with variable separation protocols. In this study, chromatographic peaks were detected by fluorescent imaging at the column outlet at a wavelength of 510 nm, but other detection modalities such as absorbance[27−29] or electrical measurements[30] are also possible. Samples are recovered by providing an alternative path at the column outlet. To minimize sample dilution, the sample plug is recovered into a flowing stream of immiscible fluorocarbon oil (FC-3283, 3M, MN) and fluorosurfactant[1] (17% 1*H*,1*H*,2*H*,2*H*-Perfluoro-1-octanol, Sigma-Aldrich) (Figure 2d).

Digital Polymerase Chain Reaction Protocol. To characterize the efficiency of our system for recovery of low

dx.doi.org/10.1021/ac400163u | *Anal. Chem.* 2013, 85, 2999−3005

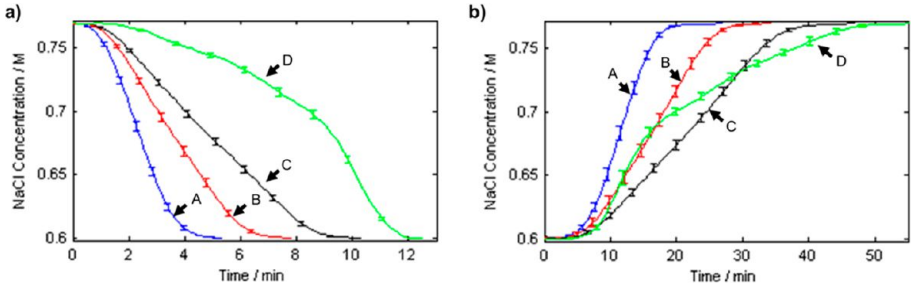

Figure 3. Measured concentration curves during gradient generation (a) and, after reversing the flow direction in the storage channel, when applied to the column array (b). Concentration curves were measured at the inlet of the gradient storage channel using absorption. Gradients were visualized by spiking buffer B with bromophenol blue at a concentration of 200 nM. A variety of gradients with different slopes and shapes may be produced with the impedance network including linear (A–C) and nonlinear gradients (D). Gradient D was used to separate a fluorescently labeled ssDNA ladder as described in the text.

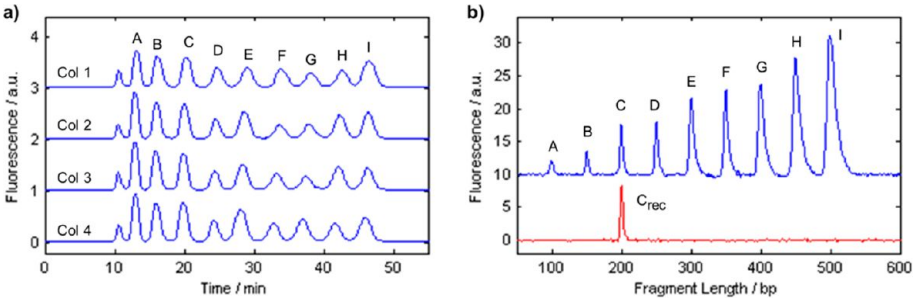

Figure 4. (a) Chromatograms of four replicates of FAM-labeled ssDNA ranging from 100 to 500 bp in 50 bp increments (A–I). The chromatograms are preceded by a peak likely resulting from unbound fluorescein. (b) Electropherograms of the complete ladder before loading onto the microfluidic device (blue) and of a 200 bp fragment recovered from a single microcolumn. No detectable cross-contamination with neighboring peaks was observed in the recovered sample fraction.

template amounts, we performed a series of sample loading and recovery experiments using a synthetic fragment of the RPPH1 gene, followed by digital polymerase chain reaction (dPCR) analysis to accurately quantify the recovery rate, defined as the ratio of the number of molecules recovered compared to the number of molecules loaded onto the column. dPCR is a single molecule counting technique that works by partitioning a sample at limiting dilution followed by PCR amplification and end point detection, to identify the presence or absence of template molecules in each reaction, and calculation of the template concentration according to a binomial distribution across the array.[31]

Following recovery of the synthetic fragment from the microcolumn, 2 μL of the sample was combined with 8 μL of PCR mix (final composition: 50% 2× TaqMan Fast Universal PCR Master Mix (Life Technologies, CA), 20% sample, 800 nM primers (Integrated DNA Technologies), 250 nM probe (Biosearch Technologies, CA), 0.1% v/v Tween 20 (Sigma-Aldrich, MO)). 1 μL of this was then loaded onto a microfluidic digital PCR array consisting of 765 1 nL chambers.[32] Following sample loading and partitioning by valve actuation, the device was transferred to a microfluidic PCR instrument for thermocycling and fluorescent imaging of the array (Prototype version of Biomark Instrument, Fluidigm). The thermocycler protocol included a 2 min hot start at 95 °C, followed by 40 cycles of 92 °C for 5 s and 60 °C for 30 s. Fluorescent imaging was performed at cycle 40.

EXPERIMENTAL RESULTS AND DISCUSSION

Devices for nucleic acid separation were prepared by parallel packing of four microcolumns with AEX resin. This resin interacts with negatively charged DNA through monovalent quaternary ammonium functional groups displayed at the bead surface. Since the overall negative charge of each DNA fragment is proportional to its length, the application of an increasing salt gradient results in elution of progressively longer fragments, thereby permitting separation according to molecular weight. We performed three experiments designed to demonstrate high-resolution separation, high-capacity sample binding and purification, and high-yield recovery of low-abundance DNA sequences. These include (1) gradient separation and recovery of a single-stranded DNA ladder (ssDNA, 100–500 bp) labeled with 6-carboxyfluorescein (FAM), (2) purification and recovery of reverse transcription (RT)-PCR amplified antibody genes, and (3) low-abundance template binding, elution, and recovery followed by digital PCR analysis to determine the sample recovery rate.

Gradient Separation and Size Selection. *Gradient Generation.* Reliable chromatographic separation requires the applied gradient to be highly reproducible and well controlled. We performed measurements to show that our resistor network design is capable of producing a wide range of gradient shapes and slopes (Figure 3). Gradients were visualized by spiking buffer B with bromophenol blue at a concentration of 200 nM. Using absorbance at a wavelength of 600 nm, the bromophenol blue concentration was determined using Beer–Lambert Law $-\log(I/I_0) = \varepsilon hc$ where I_0 and I are the transmitted intensity through buffer A and through a mixture of buffer A and buffer B, respectively; ε, h, and c represent the extinction coefficient, the channel height, and the concentration, respectively.

The concentration profile was determined at the inlet of the gradient storage channel at the time of gradient generation and

dx.doi.org/10.1021/ac400163u | *Anal. Chem.* 2013, 85, 2999–3005

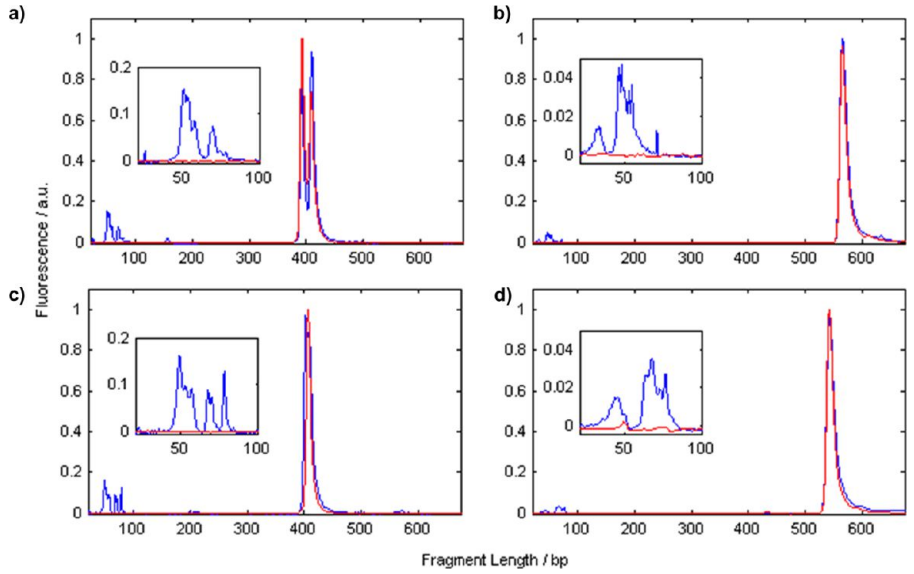

Figure 5. Electropherograms of four PCR products before (blue) and after (red) multiplexed sample purification on-chip. The following regions were amplified: (a) D1.3-kappa, (b) D1.3-heavy, (c) HyHel-5-kappa, and (d) HyHel-5-heavy. Samples were purified on-chip in parallel by application of a 0.75 M NaCl step gradient and recovered in an immiscible oil phase for off-chip analysis. The purified sample showed no detectable carry-over of PCR byproducts demonstrating efficient sample purification.

during application of the gradient to the column array following reversal of the flow direction. It was found that low flow rates, ~0.5 μL/min, resulted in gradients that accurately matched the programmed profiles, while gradient deviations were observed at higher flow rates due to Taylor dispersion effects along the storage line during gradient transport. At low flow rates, all gradients produced were accurate over the functional range of 5% to 95% mixing ratios, beyond which errors increased; buffer compositions and linear velocities were chosen to ensure that operation occurs within this linear regime.

Sample Separation and Recovery. Following column equilibration, 400 pg of FAM-labeled ssDNA ladder (100–500 bp, Bioventures, TN) was loaded onto each column in buffer A and the column then washed (5 column volumes) with buffer A. A gradient ranging from 0.6 to 0.77 M NaCl was then generated using the resistor network, stored in the storage channel, and applied to all four chromatography columns at a flow rate of 70 nL/min per column for 40 min. Imaging of the column outlets was used to generate fluorescent chromatograms for each column. In the current experimental setup, the detection area is defined by the field of view of a microscope objective and is limited to one column outlet. To demonstrate the performance of all columns, we repeated this experiment four times to sequentially record chromatograms for each column. Figure 4a shows results for the gradient separation of nine FAM-labeled ssDNA fragments, ranging from 100 to 500 bp in 50 bp increments, across four separate columns. Near baseline resolution was achieved by applying a regressive gradient ranging from 0.6 to 0.77 M NaCl. These experiments demonstrate the integration of parallel on-chip chromatography with high separation efficiency as well as excellent reproducibility in peak heights and retention times.

We then used our microfluidic system to demonstrate automated selection and recovery of eluted ssDNA strands of specific size using valves downstream of the column to collect a defined fraction of the sample into a sample collection stream. 6 ng of the ssDNA ladder was loaded, and the components were separated by applying a salt gradient as described above. While in this study fluorescence detection was used to trigger valves at the column outlet to selectively recover a fraction of the eluent containing the purified 200 bp strand, timed valve actuation may also be employed. To maintain a high concentration of the purified band, the collected fraction was injected into a stream of immiscible oil (FC-3283) and diluted to a total aqueous volume of 3 μL to facilitate off-chip handling. Following recovery from the chip, the aqueous and immiscible phases were then separated using centrifugation and the lighter aqueous phase was removed using a pipet. The strand sizes within the recovered fraction were analyzed using a commercially available microfluidic electrophoretic system (Bioanalyzer 2100, Agilent, CA) to confirm that there was no cross contamination from the neighboring bands (150 and 250 bp) (Figure 4b). On the basis of this result, we find that full resolution of ssDNA differing in size by ±20 bp can be obtained, which is comparable to the resolving power achieved by excision of conventional gel bands.

Purification of RT-PCR Amplified Antibody Genes. On-chip DNA separation is of high interest for upstream amplification applications such as sequencing library preparation or cloning. To highlight this, we applied our system to a routine sample preparation application: post-PCR amplicon purification to remove primers and PCR byproducts such as primer dimers. Variable regions of antibody heavy and light (kappa) chain genes were amplified by RT-PCR of purified RNA obtained from two mouse hybridoma cell lines (D1.3 and HyHEL-5). The expected RT-PCR products included 4 different amplicons ranging from 392 to 543 bp. Unpurified PCR amplification products were diluted 10-fold with buffer A, and 150 ng was loaded onto each column. Following a column wash, a step elution was applied at a constant NaCl concentration of 0.75 M, which from our gradient studies was known to elute oligonucleotides having lengths below 300 bp. The step profile was created by the gradient generator, stored in the gradient storage line, and applied to the column array at a flow rate of 183 nL/min/column for 10 min. As expected, fragments below 300 bp in length were effectively

dx.doi.org/10.1021/ac400163u | *Anal. Chem.* 2013, 85, 2999–3005

released from the column and discarded. Next, we created and applied a second step elution of 1 M NaCl to recover the desired PCR products, which were collected in four separate FC-3283 oil streams. Electropherograms were produced for all samples prior to loading onto the column array and for each eluted fraction (Figure 5). Integration of efficient and simple size selection of amplified DNA products, as demonstrated here, should be of high interest for low template sequencing library preparation where advantages of low elution volume, high product concentrations, and high recovery rates are required.[1,2]

Digital PCR to Assess the Sample Recovery Rate. To assess recovery rates, 200 fg of a synthetic fragment of the RPPH1 gene was loaded onto one of the columns in buffer A, rinsed, and recovered in an FC-3283 oil stream by applying 0.8 M NaCl at a flow rate of 183 nL/min. The sample was diluted on-chip by a factor of one hundred and then recovered for dPCR analysis as described above.

Three replicates of the digital PCR response from a single column are shown in Figure 6. The original sample, diluted in the same way as the eluted samples, resulted in 148/765 positive chambers. By comparison, the three eluted samples resulted in 135/765, 136/765, and 139/765, respectively, while the no-template control (NTC) did not produce any positive PCR reactions. Assuming a Poisson distribution of molecules in each chamber, the observed frequency of amplification from the initial sample corresponds to a best estimate of the concentration of λ = 0.22 molecules/nL. Using this value, we constructed a 95% confidence interval for the binomial response to be between 127 and 171 positive reactions, which includes all observed samples.[32] Although the eluted samples were not significantly different from 100% recovery, the dPCR measurements were consistently lower than that of the initial sample with an average frequency of 136.7/765. From this, we calculate the best estimate of concentration as 0.20 molecules per chamber, corresponding to a recovery rate of 91% ± 2%.

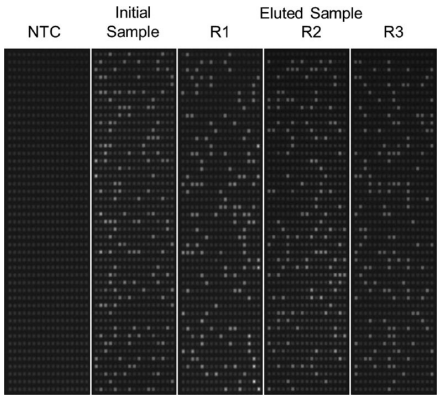

Figure 6. Fluorescent micrograph of five digital PCR arrays comparing the amount of the recovered fraction of the synthetic fragment of the RPPH1 gene (R1-R3) to the amount loaded onto one of the microcolumns. The frequency of positive wells for the initial sample and the three eluted samples are 148/765, 135/765, 136/765, and 139/765, respectively. The corresponding 95% binomial confidence intervals are 0.1660 to 0.2233, 0.1501 to 0.2054, 0.1513 to 0.2067, and 0.1550 to 0.2109, respectively. The three replicates are within 2% of the mean (91%) indicating excellent run-to-run reproducibility as well as a high level of recovery.

CONCLUSION

We have presented the first parallel and fully integrated microfluidic solid-phase chromatographic system containing all elements for sample loading, gradient generation and mixing, parallel sample separation, and fraction recovery with high yield and low dilution. By combining high-performance resins with integrated microfluidic control, this system provides flexibility in addressing many different analytical and preparative separation applications. Here, using a nonporous AEX resin, we demonstrate the size-based separation and selective recovery of low molecular weight DNA fragments, achieving performance comparable to what is possible using standard gel electrophoresis methods. We further show how the columns may be integrated with important sample preparation steps to permit, for example, the parallel purification and size-selective recovery of PCR amplification products. Although not demonstrated here, we expect this functionality to be important for enabling the transfer of multistep genomics protocols onto a chip format. Importantly, our system enables the reproducible processing of low abundant template samples with minimal losses, achieving recovery rates in excess of 90% as measured by digital PCR. We expect that the integration of high performance sample separation methods will greatly expand the range of applications for MSL-based microfluidics, with applications including small volume sequencing library production, proteomic analysis, sample preparation for diagnostics, and miniaturized chemical synthesis.

ASSOCIATED CONTENT

Supporting Information

Additional information as noted in text. This material is available free of charge via the Internet at http://pubs.acs.org.

AUTHOR INFORMATION

Corresponding Author

*E-mail: chansen@phas.ubc.ca. Fax: +1 604-822-2114.

Notes

The authors declare no competing financial interest.

ACKNOWLEDGMENTS

This research was funded by the Canadian Institute for Health Research (CIHR Catalyst Grant) and the Natural Sciences and Engineering Research Council of Canada (NSERC Discovery and GSAT CREATE grants). We also acknowledge Genome British Columbia and Western Economic Diversification Canada for infrastructure support. Finally, C.L.H. thanks the Michael Smith Foundation for Health Research and CIHR for career salary support.

REFERENCES

(1) Leung, K.; Zahn, H.; Leaver, T.; Konwar, K. M.; Hanson, N. W.; Pagé, A. P.; Lo, C.; Chain, P. S.; Hallam, S. J.; Hansen, C. L. *Proc. Natl. Acad. Sci.* **2012**, *109* (20), 7665−7670.

(2) White, A. K.; VanInsberghe, M.; Petriv, O. I.; Hamidi, M.; Sikorski, D.; Marra, M. A.; Piret, J.; Aparicio, S.; Hansen, C. L. *Proc. Natl. Acad. Sci.* **2011**, *108*, 13999−14004.

(3) Lee, C.; Snyder, T. M.; Quake, S. R. *Nucleic Acids Res.* **2010**, *38* (8), 2514−2521.

(4) Zhou, X.; Cai, S.; Hong, A.; You, Q.; Yu, P.; Sheng, N.; Srivannavit, O.; Muranjan, S.; Rouillard, J. M.; Xia, Y.; Zhang, X.; Xiang, Q.; Ganesh, R.; Zhu, Q.; Matejko, A.; Gulari, E.; Gao, X. *Nucleic Acids Res.* **2004**, *32* (18), 5409−5417.

(5) Kong, D. S.; Carr, P. A.; Chen, L.; Zhang, S.; Jacobson, J. M. *Nucleic Acids Res.* **2007**, *35* (8), No. e61.
(6) Moon, H.; Wheeler, A. R.; Garrell, R. L; Loo, J. A.; Kim, C. J. *Lab Chip* **2006**, *6*, 1213−1219.
(7) Lion, N.; Rohner, T. C.; Dayon, L.; Arnaud, I.; Damoc, E.; Youhnovski, N.; Wu, Z.; Roussel, C.; Josserand, J.; Jensen, H.; Rossier, J. S.; Przybylski, M.; Girault, H. H. *Electrophoresis* **2003**, *24* (21), 3533−3562.
(8) Harrison, D. J.; Fluri, K.; Seiler, K.; Fan, Z.; Effenhauser, C. S.; Manz, A. *Science* **1993**, *261*, 895−897.
(9) Szumski, M.; Buszewski, B. *Crit. Rev. Anal. Chem.* **2002**, *32* (1), 1−46.
(10) Saito, Y.; Jinno, K.; Greibrokk, T. *J. Sep. Sci.* **2004**, *27* (17), 1379−1390.
(11) Yang, X.; Zhang, X.; Li, A.; Zhu, S.; Huang, Y. *Electrophoresis* **2003**, *24* (9), 1451−1457.
(12) Trojanowicz, M. *Anal. Chim. Acta* **2009**, *653*, 36−58.
(13) Kohlheyer, D.; Eijkel, J. C.; van den Berg, A.; Schasfoort, R. B. *Electrophoresis* **2008**, *29*, 977−993.
(14) Yin, H.; Killeen, K. *J. Sep. Sci.* **2007**, *30*, 1427−1434.
(15) Lee, J.; Soper, S.; Murray, K. *J. Mass Spectrom.* **2009**, *44*, 579−593.
(16) Yin, H.; Killeen, K.; Brennen, R.; Sobek, D.; Werlich, M.; van de Goor, T. *Anal. Chem.* **2005**, *77*, 527−533.
(17) Jemere, A. B.; Oleschuk, R. D.; Harrison, D. J. *Electrophoresis* **2003**, *24*, 3018−3025.
(18) Oleschuk, R. D.; Shultz-Lockyear, L. L.; Ning, Y.; Harrison, D. J. *Anal. Chem.* **1999**, *72*, 585−590.
(19) Ceriotti, L.; de Rooij, N. F.; Verpoorte, E. *Anal. Chem.* **2002**, *74*, 639−647.
(20) Gaspar, A.; Hernandez, L.; Stevens, S.; Gomez, F. A. *Electrophoresis* **2008**, *29*, 1638−1642.
(21) Gaspar, A.; Piyasena, M. E.; Gomez, F. A. *Anal. Chem.* **2007**, *79*, 7906−7909.
(22) Huft, J.; Haynes, C. A.; Hansen, C. L. *Anal. Chem.* **2013**, *85*, 1797−1802.
(23) Thorsen, T.; Maerkl, S. J.; Quake, S. R. *Science* **2002**, *298*, 580−584.
(24) Unger, M.; Chou, H.; Thorsen, T.; Scherer, A.; Quake, S. R. *Science* **2000**, *288*, 113−116.
(25) Huft, J.; Da Costa, D. J.; Walker, D.; Hansen, C. L. *Lab Chip* **2010**, *10* (18), 2358−2365.
(26) Rolland, J. P.; Van Dam, R. M.; Schorzman, D. A.; Quake, S. R.; DeSimone, J. M. *J. Am. Chem. Soc.* **2004**, *126*, 2322−2323.
(27) Fritzsche, W.; Taton, T. A. *Nanotechnology* **2003**, *14*, R63.
(28) Mogensen, K. B.; Eriksson, F.; Gustafsson, O.; Nikolajsen, R. P. H.; Kutter, J. P. *Electrophoresis* **2004**, *25*, 21−22.
(29) Malcik, N.; Ferrance, J. P.; Landers, J. P.; Caglar, P. *Sens. Actuators, B: Chem.* **2005**, *107*, 24−31.
(30) Cui, Y.; Wei, Q.; Park, H.; Lieber, C. M. *Science* **2001**, *293*, 1289−1292.
(31) Vogelstein, B.; Kinzler, K. W. *Proc. Natl. Acad. Sci.* **1999**, *96*, 9236−9241.
(32) Warren, L. A.; Weinstein, J. A.; Quake, S. R. *The Digital Array Response Curve*; 2007. Available: http://thebigone.stanford.edu/papers/Weinstein%20DigResCurve.pdf. Accessed 21 Nov 2012.